Single Event Effects from Ions Produced in Nuclear Reactions of CMOS with Cosmic Rays

William J Atkinson, Senior Member IEEE
William.J.Atkinson2@boeing.com
The Boeing Company
P.O. Box 240002, 48-18.2, 3016, Mail Code JW-153
Huntsville, AL. 35824-6402

1. Introduction

Single Event Effects (SEEs), disruptions in a microelectronic device caused by the passage of an energetic particle through the sensitive region of the device, are an increasing problem with advances in technologies. Three technology trends are responsible for the increased number of SEEs over the last decade. First, with the reduction of the operating voltages, devices have are susceptible to smaller amounts of radiations. Secondly, the data densities (bits per device) increased dramatically to meet the demand for more memory and faster processing time. Thirdly, commercial electronics firms have lowered the priority of radiation hardness in order to reduce manufacturing costs. Memory cells have received more attention than those in latches and combinatorial logic simply because there are more memory cells than the other types of cells. However, with the continued trends in technology, analyses by Shivakumar *et. al.* demonstrated that by 2011 SEEs of combinatorial logic will become comparable to that of unprotected memory elements.[1]

There are three categories of SEEs based on the level of disruption to the device [2]:

1. Single event upset (soft error) ,
2. Single event latchup (soft or hard error),
3. Single event burnout (hard failure).

Single Event Upsets (SEUs) are changes in the logic state of a cell. An SEU usually disappears after rewriting to the affected bits. Consequently, SEUs are categorized as *soft errors*. This condition results when the charge deposited in a cell exceeds a threshold value referred to as the *critical charge*. If the particle energy is high enough, more than a single bit is affected resulting in a Multiple Bit Upset (MBU). While the opportunity of a multiple bit upsets is low compared to an SEU, their occurrence has implications in memory systems using Error Correction and Detection (EDAC) [3, 4]. In a Single Event Latchup (SEL), the device ceases to function due to a particle strike producing a large surge of current. Kolasinski et al. first observed SELs in 1979 during ground testing [5]. An SEL can also be a *hard error* causing permanent damage to the device. The latched condition can destroy the device, drag down the bus voltage, or damage the power supply. The practice for eliminating a SEL is resetting the power to the device. A Single Event Burnout (SEB) is a *hard error* that can cause permanent device destruction due to a current state exceeding the specifications of the device. SEB of power MOSFETs was first reported by Waskiewicz *et al.* in 1986[6]. Only SEB of n-channel power MOSFETs has been reported[7]. A power MOSFET may undergo *single-event gate rupture* (SEGR), the formation of a conducting path (localized dielectric breakdown) in the gate oxide resulting in a destructive burnout. Fischer was the first to report on SEGR of power MOSFETs in 1987[8]. A SEB can also occur in bipolar junction transistors (BJTs) as was first reported by Titus *et al.* in 1991[9].

The earliest reports on SEEs were observed in space systems in 1975[10]. The

radiations responsible for SEEs in space are proton, alphas (helium nuclei), and heavy ions (nuclei with an atomic number greater than 2). It took fifteen more years for SEEs to be recognized as a problem affecting avionic systems. Approximately 97% of the SEEs at avionic altitudes (15000-55000 ft) and terrestrial altitudes (up to 15000 ft above mean sea level) are attributed to *atmospheric neutrons*. Atmospheric neutrons are produced by nuclear reactions of ions in cosmic rays with atoms in the atmosphere[11].

In this paper, the Soft Error Rates (SERs) in microelectronic devices in space and in the atmosphere were computed using a model developed at Boeing, TSAREME (Total Space and Atmospheric Radiations Effects on Microelectronics). In space, the incident radiations TSAREME modeled were protons, alphas, and heavy ions with an atomic number as high as 26 (iron). In the atmosphere, the incident radiations TSAREME modeled were atmospheric neutrons produced by nuclear reactions of ions with atoms in the atmosphere. The reactions products of the incident radiations with materials of the device model included neutrons, protons, and heavy ions with atomic numbers as high as 26 (iron), high speed electrons, gamma rays and x-rays.

In space, the SER is computed in two devices of similar structure. The first device is a 4 Mbit 2 micron Complementary Metal Oxide on Semiconductor (CMOS) described in [12]. The second device is the first device with aluminum and tantalum shielding and an overlayer of Borophosilicate glass (BPSG). A comparison of the SER generated for these devices indicated that metallic shielding and BPSG increased the SER from zero to 80 upsets per day. In the atmosphere, the soft error rates due to atmospheric neutrons are computed in scaled submicron CMOS devices discussed in Shivakumar[1].

The rest of the paper is organized as follows. Section 2 discusses the origins and variability of radiations in space, and the many available decay paths possible as incident radiations react at the nuclear level with materials of a device. Section 3 discusses the

- models for generating typical near earth radiation environments in space as well as in the atmosphere,
- model for transporting these radiations across the various materials of the device,
- programs to compute the SER of the device from data generated by the transport model,
- detailed structures available for the devices modeled.

Section 4 gives the detailed results on the SER in space and in the atmosphere. Section 5 discusses the significance of the results reported section 4.

2. Background

A. Radiation Environments

a. Space Radiations

Radiation in space consists of protons, alpha particles, and heavy ions originating from solar flares and from galactic sources. The radiation from the sun, known as Solar Cosmic Rays (SCR) varies with time over an 11 year cycle as observed in Figure 1. Note the three prominent solar flares. The solar flares occurring October 19, 1989 was categorized by the JPL model as the '99% worst solar flares' based on the fluence measured at three proton energies: 10, 30, and 60 MeV. The proton fluence for the August 4, 1972 solar flare ranked in the 99% worst flare based on fluence at energies of 10 and 30 MeV but not the 60 Mev energy[14] The Feb. 23, 1956 incident was not evaluated due to lack of fluence data.

The solar flare of October 19, 1989 is often used as a test case in modeling radiation hardening of space based systems. Models that include the October 19, 1989 test case include the

- Cosmic Ray Effects on Microelectronics, version 1996 (CREME96) [15]
- Modeling and Analysis of Cosmic Ray Effects in Electronics (MACREE) developed by Boeing to refine predictions of the SER in the Space Station[16].

It is generally concluded that protons as well as heavy ions must be considered together in accurately determining SEU vulnerabilities as illustrated[14]. This conclusion rests on two contrasting cases. Evaluations in [14,15] show that at least 45% of the SEUs in the October 19, 1989 solar flare were produced predominantly by heavy ions. In contrast, the SEU rates examined for a separate event in device (AMD931L422 on LEASATs) indicated that SEUs were overwhelmingly due to protons.[14]

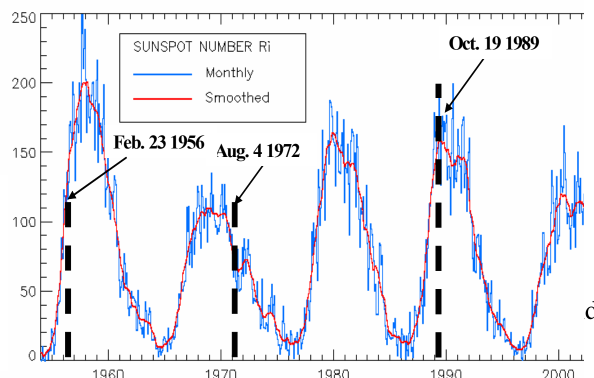

Environmental Satellite (GOES) monitor[13]

b. Avionic Radiations

Protons and heavy ions in cosmic rays entering the atmosphere produce a "shower" of *secondary* particles throughout the atmosphere as shown in see Figure 2. These particles decay to other particles in three major chains:

1. nucleonic component consisting mostly of protons and neutrons,
2. meson "hard" component consisting of pions and muons,
3. electromagnetic "soft" component consisting of gamma rays, electrons, and positrons.

As noted in Figure 2, a fraction of the nucleons can decay to mesons and to a lesser extent mesons decay to nucleons. Nucleonic decays dominant all of these decay chains[17]. Neutrons are identified as the primary cause of SEEs at avionic altitudes[18, 19]. As indicated in Figure 3, neutrons can have energies that well exceed 1000 MeV.

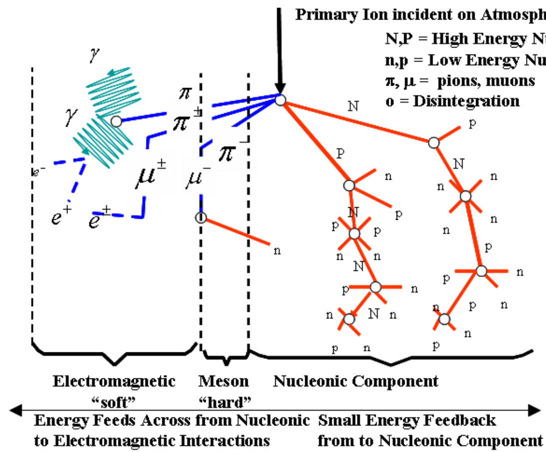

Figure 2. Cosmic ray shower produced by heavy ions incident on atmosphere.

The neutron flux varies with altitude and latitude as shown in Figure 4, peaking in altitude at approximately 60000 ft. The peak in the number of neutrons is due to scattering and absorption of neutrons in the atmosphere. The number of secondary neutrons scattered down into the atmosphere builds up the deeper the atmosphere is penetrated. At the same time, neutrons (primary and secondary) are absorbed in the atmosphere with increasing depth into the atmosphere as a result of the increase in air density with decreasing altitude. The point where the neutron flux peaks represents the altitude where the neutrons scattered just equals the neutrons absorbed. Also note in Figure 4 that the flux at the poles is five times that at the equator. This is a result of the magnetosphere being weaker at the poles than at the equator thus allowing ions in cosmic rays to penetrate further into the atmosphere at the poles than at the equator.

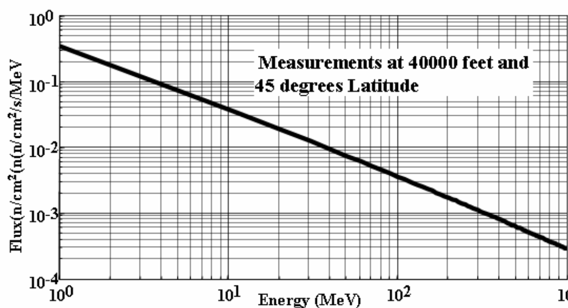

Figure 3. Neutron spectrum at 40,000 ft. and 45° latitude[18,19].

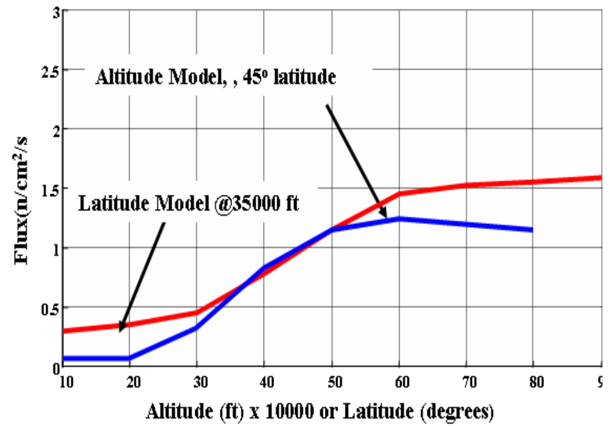

Figure 4. Neutron flux versus altitude[18] and altitude[19, 20].

A model used in past investigations[17] is to express the neutron flux at an arbitrary energy, altitude, and geographic latitude as separable functions of these three variables utilizing the information in Figures 3 for the energy dependence and Figure 4 for the altitude and latitude dependence.

c. Terrestrial Radiations

Neutrons are considered the major contributor to SEEs on the ground. The flux of neutrons at ground is about 1/300 of that at 40000 ft. Information from Figures 3 and 4 can be used to compute the neutron flux at terrestrial altitudes with adjustments made for the elevation above mean sea level[11]. Computer systems on the ground with the highest measured SEU rates are ones with a large amount of memory. The ACPMAP5 computer system at the Fermilab contains about 160 Gbits of DRAM memory. Based on errors logged over a period of many months, the system averaged about 2.5 upsets per day[21].

B. Reactions of Radiations with Device

Consider now the nuclear reactions between radiations and the materials in a microelectronic device. Figure 5 illustrates two possible reactions between silicon and an incident neutron at the top of Figure 5 and two possible reactions between silicon and a proton in the middle of Figure 5. Other reaction paths are possible other than these two paths. Also, the incident particle may be an alpha or heavy ion, or possibly an electron (beta particle). At

the bottom, second generation reaction products are shown beginning with a reaction between a proton and silicon. The proton and aluminum ions produced in the first generation react to give a magnesium ion and an alpha in the second generation. All of these reaction products other than neutrons deposit electromagnetic energy into silicon. A portion of this deposited energy is used to produce charge as electron-hole pairs in silicon. One quickly sees that tracking the many possible reaction paths over muliple generations of decay and accurately determining the yields, trajectories, energies, and energy deposition of each particle produced in each generation is a task possible only with large computer resources and well validated software for modeling the transport of the many possible types of particles.

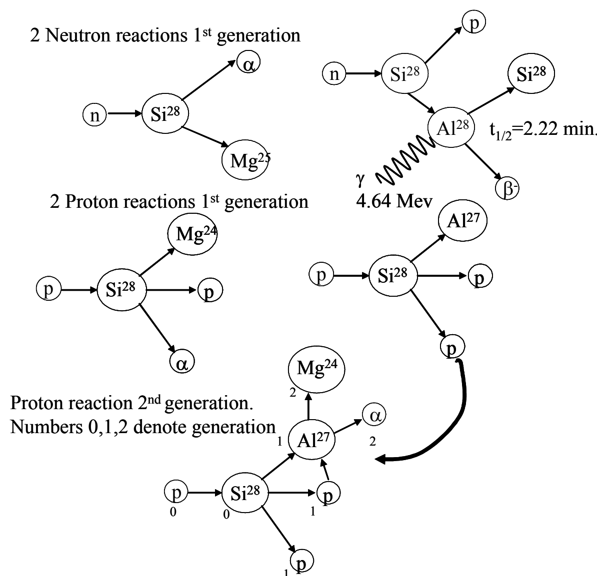

Figure 5. Nuclear reactions of protons and neutrons with silicon showing 2nd generation products for one reaction.

3. Methods

Figure 6 shows the three primary software modules in the TSAREME. The modules are:

1. code generating fluxes of incident particles expected in either space or in the earth's atmosphere,
2. code transporting the particles through various materials and possibly deposited in the sensitive volume of a cell,
3. code computing the single event upset cross section per cell and the SER.

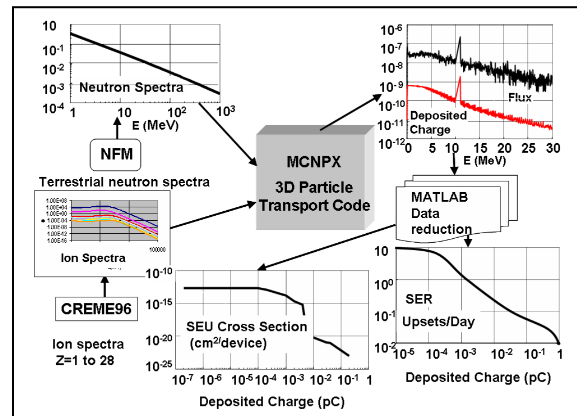

Figure 6. Modules, inputs, and outputs of TSAREME.

A. Particle Flux Evaluation

The model for computing the particle distributions depends on the location of the microelectronic device. For a device in a near earth orbit where the particles are protons and heavy ions, the fluxes of the particles are computed over the entire energy spectrum by the CREME96. The various modules of CREME96 are described in Figure 7. Critical to computing proton and ion fluxes are the range in the atomic number (Z) of the ions and the solar period. The two extreme test cases of the solar period in CREME96 are:

1. solar minimum and Galactic Cosmic Ray (GCR) maximum in 1977,
2. solar maximum and GCR minimum solar flare episode in October 19, 1989.

Three cases of the solar maximum and GCR minimum are canned in CREME96: peak week, peak day, and peak 5 minutes that averages the fluxes over 180 hours, 18 hours, and 5 minutes respectively all starting 1300 UT on 19 October 1989.

Also, as noted in Figure 7,

1. SER was not computed in the module HUP of CREME96 ,
2. radiation reduction from shielding is not computed in the module TRANS of CREME96

3. Linear Energy Transfer (LET) was not computed in LETSPEC.

The rationale for these decisions is that none of the modules in CRÈME96 account for neutrons and secondary ions.

For a device at avionic altitudes, the incident neutron flux at the surface of the aircraft is computed as discussed in earlier (2.B.b) and 2.B.c). These neutron flux spectra are then provided as inputs into the radiation transport code of TSAREME

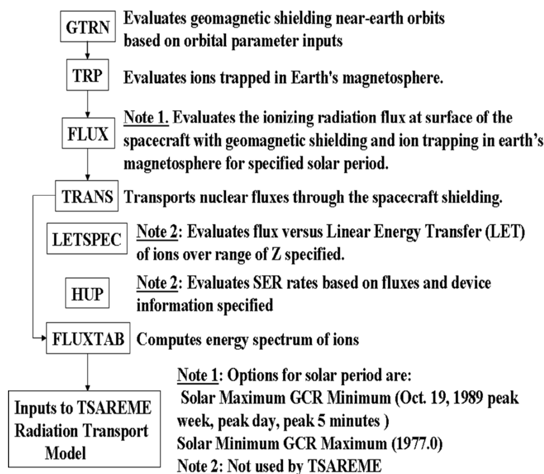

Figure 7. Preparing input ion spectra to TSAREME transport model using CREME96.

B. Radiation Transport Code

The radiation transport code used in TSAREME was MCNPX. MCNPX is a general-purpose Monte Carlo radiation transport code for modeling the interaction of radiation with all types of material. MCNPX stands for Monte Carlo N-Particle eXtended. MCNPX extends the capabilities of MCNP5P1 from just neutrons, electrons, and photons to nearly all particle types, to nearly all energies, and to nearly all applications without additional computational time. MCNPX is fully three-dimensional and time dependent. The code utilizes the latest nuclear cross section libraries and uses physics models for particle types and energies where tabular data are not available. Applications range from outer space (the discovery of water on Mars) to deep underground (where radiation is used to search for oil.). MCNPX is used in nuclear safeguards, accelerator design and applications, nuclear reactors, radiotherapy facility design and treatment planning, active and passive detection of nuclear materials, and cosmic-ray interactions with spacecraft and planetary objects. Table 1 lists advantages of using MCNPX in studying single event effects.

Table 1. Advantages of Heavy Ion MCNPX

Advantages of heavy Ion Code MCNPX
Requires no software development
Addresses the particles of interest to current SEE applications (neutrons, protons, alphas, ions with Z=1 to 100, and electrons) as well as possible future ones (pions, muons).
Modeling devices in 3D.
Excellent documentation
Software and documentation free (information public domain)
Forum where users can exchange information with other users via electronic mail.
Workshops at levels ranging from introduction to advance applications.
Extensive up to date cross section data for materials of interest in SEEs : all isotopes of silicon, boron, various metals.
Computes cross sections of mixtures and compounds given the composition specified by the MCNPX user.
Modeling multiple cells. Applications include computing probabilities of Multiple Bit Upsets (MBUs) and also charge sharing among cells.
"Tally" variables of interest to a range of investigators. Tallies used in TSAREME were energy deposition of particles and their fluxes.
Collection of particle coincidence data. This type of data application to examining MBUs.
Alternatives to the continuous slowing down approximation used by CREME96 in modeling energy straggling. A good model for energy straggling is necessary to accurately compute the deposited energy (and thus deposited charge). The one recommended in MCNPX manual is the Vavilov approximation[22]

MCNPX allows the user to model the geometries and materials in devices as detailed as the one shown in Figure 8. The ability to actually model the device therefore is limited

only by the information one exacts from the specific foundry. Figure 8a shows the three major sections of the MCNPX inputs in TSAREME. The first section defines volumes or 'cells' in terms of surfaces and the materials composing each cell. A variety of surfaces can be modeled in MCNPX, a full description of which can be found in [23]. The materials can be elements such as silicon, compounds such as BPSG or ceramic, or mixtures such as air. Specifications for the cells, surfaces, and materials depend, of course, on the specific device. The next section of inputs, the source distribution (SDEF), defines the distribution of the incident particles. In space, the particle distributions are the flux versus energy of ions over a range of atomic numbers specified by the user. These distributions are the outputs of the FLUXTAB module of CREME96 (see Figure 7). In the atmosphere, the particle distributions are the neutron flux versus energy obtained from module NFM of TSAREME (see Figure 6). The tallies section of the MCNPX file gives information of the cells and surfaces where measurements of quantities specified by the user are recorded. Note that the 'raw' tally values F2 and F6 are computed per source particle, the units for F2 being particles/cm^2/s/source particle and F6 being MeV/g/source particle. The conversions necessary to compute the total particles produced in the sensitive volume of the cell at a given energy E, $N_S(E)$, and the total charge deposited by all these particles volume at a given energy E, $Q_T(E)$, are:

$$N_S(E) = [A_c \Phi_i A_s] F2 \quad (1)$$

$$Q_T(E) = \left[\frac{0.1602 A_c \Phi_i \rho_s V_s}{W_{ehp}} \right] F6 \quad (2)$$

where A_c and A_s denote the area of incidence of the cell and sensitive volume, Φ_i denotes the incident flux, ρ_s and V_s denote the density and volume of the sensitive cell, and W_{ehp} denotes the energy in MeV needed to produce an electron-hole pair, and the energy dependence in tallies F2 and F6 are understood. The conversions of the raw tallies (F2 and F6) are done internally in MCNPX by specifying values of the bracketed terms in equation (1) and (2) as the parameter values in MCNPX 'EM card'. Table 2 gives the values of W_{ehp} and densities representative of materials in many microelectronics components needed to perform the conversions. The density W_{ehp} and for silicon (3.6 eV) was used in this paper. The variables $N_S(E)$ and $Q_T(E)$, shown in Figure 9 as a function of the ion energy, indicates the ions produced primarily have energies less than about 11 MeV

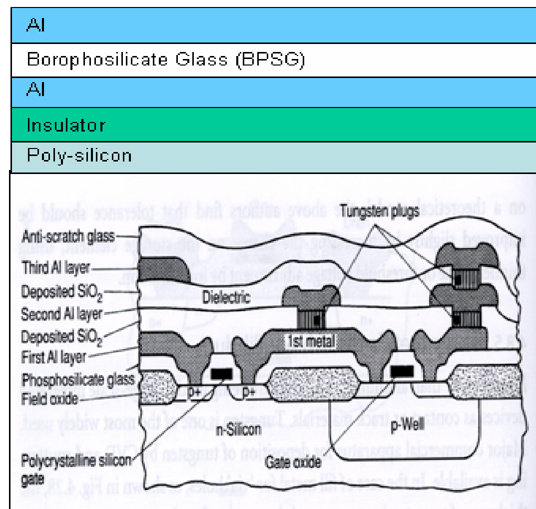

Figure 8. Detailed structure of microelectronic device that can be modeled with MCNPX.

Section	Notes
Cells – defines volumes via surfaces and materials in volumes Surfaces – A set of surfaces, along with materials, define the cell Materials – elements such as Si or compounds such as BPSG or ceramic.	Values based on specific Device.
SDEF – define spectrum of source: ions or neutrons, i. e., flux versus particle energy	Output from CREME96 (space) or NFM (atmosphere)
Tallies – Values averaged over many runs. Current tallies are flux (F2) and energy deposition (F6) tallies, and mesh tallies of flux and energy deposition.	Grid and limits on energy fairly standard between runs though cells and surface assignments vary with specific device.

Figure 8a. Sections of MCNPX input file.

Table 2. Densities and energies needed to produce an electron-hole pair in various materials at 27 C (Ref. 24).

Material	Ge	Si	GaAs	SiO_2	Si_3N_4	Al_2O_3
Density (g/cm^3)	5.3	2.3	5.3	2.3	3.4	4.0
W_{ehp} (eV)	2.8	3.6	4.8	17.0	10.8	19.1

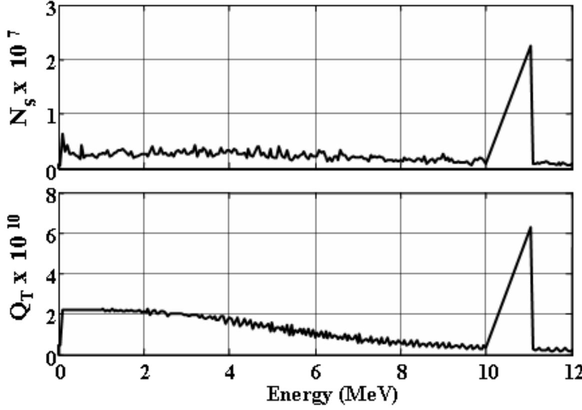

Figure 9. Number of ions (N_C) and total charge (Q_T) in the sensitive volume of SRAM obtained by TSAREME.

C. MATLAB Data Reduction

MATLAB 7.04 [25] was utilized in computing the final parameters characterizing radiation hardness of an electronic device, graphics, and manipulations of the output files generated by MCNPX. The two functions computed in the MATLAB programs developed to measure resilience of a device to radiation are the SEU cross section and the SER.

The SEU cross section per cell(bit) σ is computed as the total number of ions produced N_S in the sensitive volume with a deposited charge per ion Q_D exceeding a threshold value Q_C divided by the incident particle flux Φ_i. For a series of n measurements $N_S^{(j)}$ and $Q_D^{(j)}$ at energies $E_1, E_2, ...E_j, ...E_n$, the SEU cross section becomes

$$\sigma(Q_D) = \frac{\sum_{j=1}^{n} N_S^{(j)}\left(Q_D^{(j)} \mid Q_D^{(j)} > Q_C\right)}{\Phi_i}, \quad (3)$$

an expression given in[12]. Definition (3) is extended into this paper to cover computations of the SEU cross sections space systems and also systems in the earth's atmosphere. The only independent variable to (3) yet to be computed, Q_D. Q_D is computed from the number of ions produced in the sensitive volume N_S computed in MCNPX using equation (1) and the charge deposited by all of these ions Q_T as:

$$Q_D^{(j)} = \frac{Q_T^{(j)}}{N_S^{(j)}}. \quad (4)$$

With the values in equation (4) computed in MATLAB, the SEU cross section can then be computed as a function of the threshold charge. Figure 10 shows the SEU cross section per device for a device subject in space subject to GCR. The SEU cross section per device is simply the value computed from equation (3) multiplied by the data density.

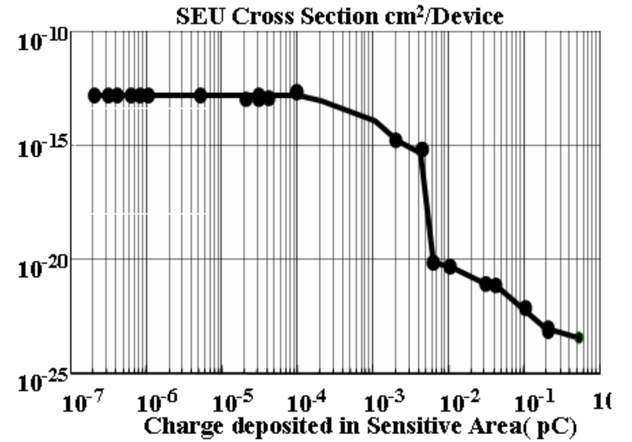

Figure 10. SEU Cross section for s device subjected to CREME96 GCR test case.

From Figure 6, one can directly compute the SEU cross section given the critical charge of the device. The SER can then computed as:

$$SER = \varepsilon\sigma\Phi_i B \quad (5)$$

where B is the data density (bits/chip) and ε is the collection charge efficiency (CCE). The CCE as originally defined by Zeigler is the fraction of ions in the sensitive volume that deposited their energy in the volume[26]. The CCE has been used since Zeigler as a parameter in computing the neutron induced

SER using the Burst Generation Rate (BGR) method [11, 27, 28].

D. Device Models

The first set of devices modeled consists of Devices A and B in Figure 11. The materials of the cell components in Device A, and the thicknesses and positions of each component in this device were based on an actual SRAM device discussed in [29]. The structure of Device B is identical to that of Device A except for the layers of aluminum and tantalum shielding and a layer of BPSG. The chemical composition of BPSG used in modeling Device B taken from [30] indicates that BPSG contains about 3% Boron-10 (B-10). The B-10 concentration in the silicon doping assumed a value 10^{19} B-10 atoms/cm^3 of silicon in the device models. The proton and heavy ion fluxes computed to these devices with CREME96 assumed an orbit with an altitude of 1800 km and an inclination of 60 degrees. Proton trapping was also included in the flux calculations. Shielding was included only for Device B. The two extremes of the space radiation environments of CREME96 provided the test cases:

- peak 5 minute solar flare of October 19, 1989,
- solar minimum and Galactic Cosmic Ray (GCR) maximum in 1977, hereafter referred to as GCR.

The flux calculations of CREME96 for protons and ions with Z between Z=2 (helium) to Z=26 (iron) were then included in the MCNPX inputs as parameters in the source distribution function (SDEF) discussed in section 3.B.

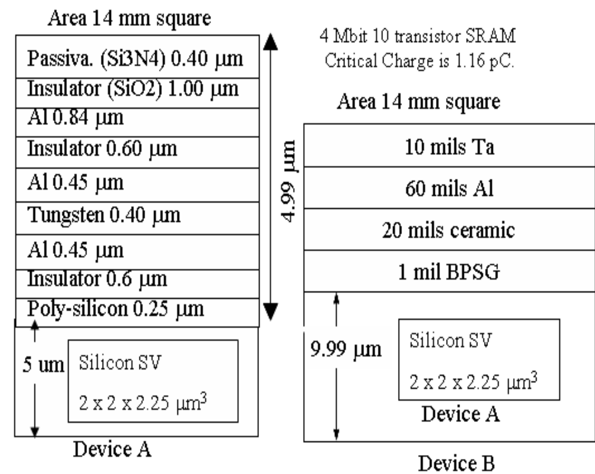

Figure 11. Device models in space environment investigations.

The other set of devices examined were submicron devices with overlayer structures similar to those of Device A but with much smaller volumes for the sensitive silicon region and surrounding silicon. As shown in Figure 12, the sensitive volume is a cube of silicon with a side length of L nanometers placed at the center of a cube of silicon with a side length of $2L$ nanometers. The dimensions of the sensitive volume, the critical charge, and the data densities were based on technology generation models from 1992 to 2011 discussed by Shivakumar et. al.[1]. The values adopted in this paper are given in Table 3.

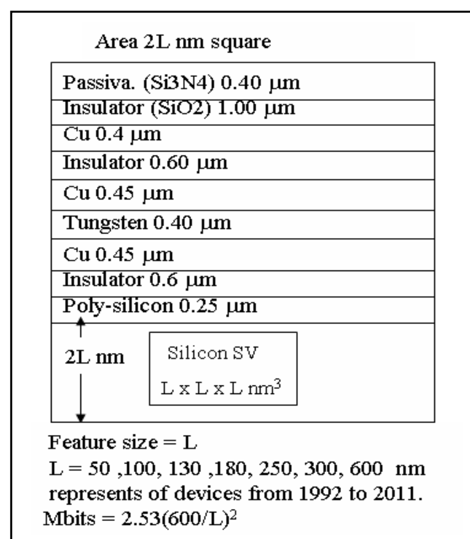

Figure 12. Device models in avionic altitude investigations.

Year	L(nm)	Q_c(fC)	Mbits
1992	600	146.0	0.86
1994	350	48.80	2.53
1997	250	33.70	4.97
1999	180	12.90	9.58
2002	130	6.31	13.79
2005	100	1.52	31.03
2011	50	0.67	124.13

Table 3. Parameters used in device models shown in Figure 12.

4. Results

One billion Monte Carlo runs were made in all MCNPX runs. This applies for all the space environment test cases (peak solar flare and GCR) and earth environments at avionic and terrestrial altitudes. The accuracy of the fluxes and energy depositions were less than 1% in all energy bins. The limits on the energy bins extended from 0.025 MeV to 50 MeV. Preliminary test runs results such as those in Figure 9 indicated that the fluxes and energy depositions at energies a high as 30 MeV were negligible. The natural relative abundances of each element were also modeled.

A. Space Environments

Figure 13 gives the SEU cross sections of Devices A and B in the peak 5 minute solar flare and GCR environments. Note that the deposited charge in the SV of Device B was always greater than that in Device A given the same space environment. Two reactions were responsible for the greater energy deposition in Device B. First, while the tantalum and aluminum layers shielded high energy ions, these metals also produced a large number of neutrons. These neutrons were indirectly responsible for the production of ions in other materials of Device B. Secondly, low energy neutrons interacted with B-10 (19.9% abundance B-10 and 80.1% B-11) in the BPSG overlayer to produce alphas and lithium ions with the release of 0.84 MeV.

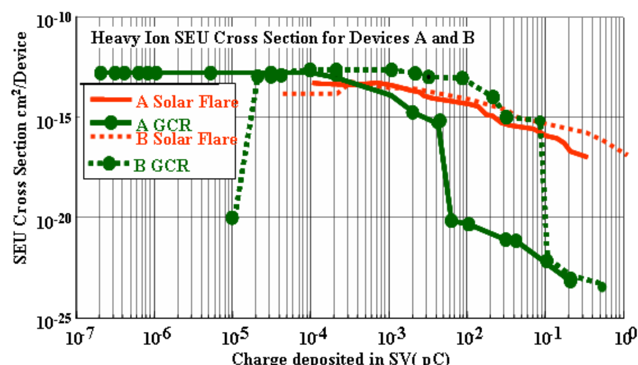

Figure 13. Heavy ion SEU cross section for Devices A and B of Figure 11.

Figures 14 and 15 give the SER of Devices A and B in the peak solar flare and GCR environments as computed by TSAREME and CREME96. The inputs to CREME96 were the critical charge covering the ranges shown in Figures 14 and 15 and the feature size. The feature size L associated with the critical charge Q_c was computed from a relationship given by Robinson et. al. valid for a wide range of device technologies [31]:

$$L(\mu m) = 6.594\sqrt{Q_c(pC)} \ . \qquad (6)$$

Three important observations can be made from Figure 14 concerning the SER of the devices in the peak 5 minute solar flare test case. First, TSAREME predicted no SEUs for device A and a SER of about 80 upsets per day for device B. Secondly, CREME96 failed to predict the SEUs predicted by TSAREME. Thirdly, TSAREME predicted charge depositions 1.14 pC higher than that predicted by CREME96. In contrast, Figure 15 shows no SEUs occurred in either device A or B when exposed to GCR. Also note that TSAREME predicted charge depositions 0.48 pC higher than that predicted by CREME96.

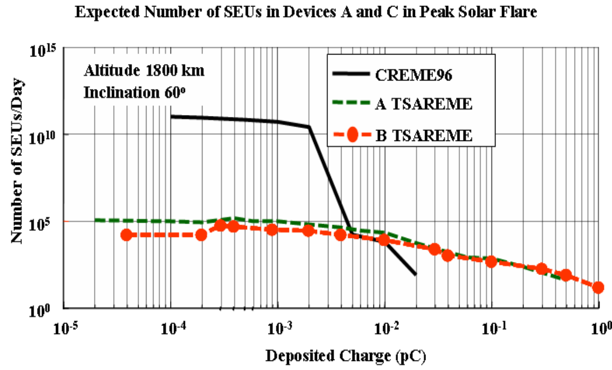

Figure 14. SER of devices A and B in solar flare computed by CREME96 and TSAREME.

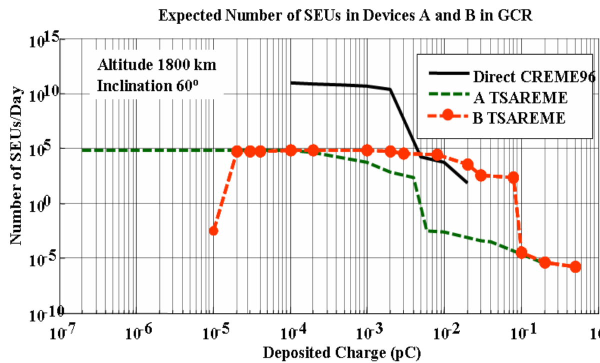

Figure 15. SER of devices A and B in GCR computed by CREME96 and TSAREME.

B. Atmospheric Neutron Environments

The SEU cross section per bit is shown in Figure 16 as a function of the feature size. Figure 17 shows the good agreement between in-flight measurements of the SER of onboard IMS 1602 SRAM (feature size 1.3 µm) discussed in[11] and the upsets/bit/hr in a CMOS models computed by TSAREME. While the SEU cross section decreases with decreasing feature size, the SER per device increases with decreasing feature as illustrated in Figures 18 through 20. Figure 20 indicates that 100 nm devices can experience as many as 9.8 upsets per day and that 50 nm devices 11.6 upset per day at northern latitudes. At the equator, the error rates for 50 nm and 100 nm devices drop off by a factor of 5 to only 2.0 and 2.3 upsets per day respectively.

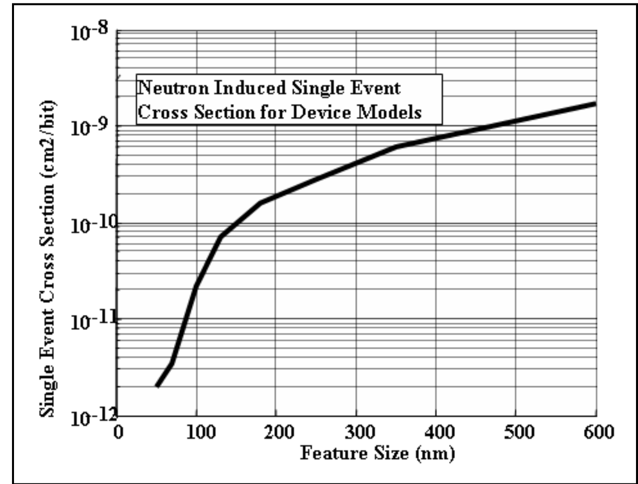

Figure 16. Neutron induced SEU cross section versus feature size of CMOS Device.

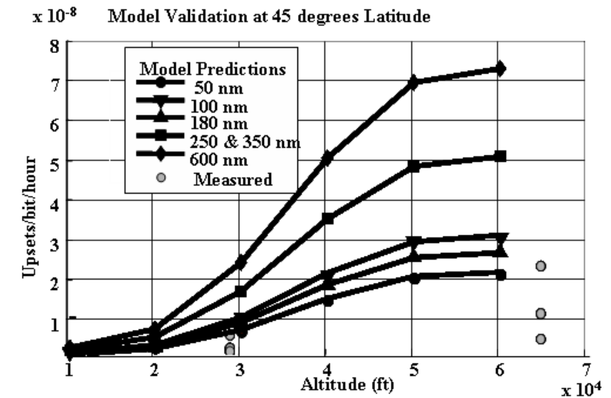

Figure 17. TSAREME calculations validated by flight measurements in [11].

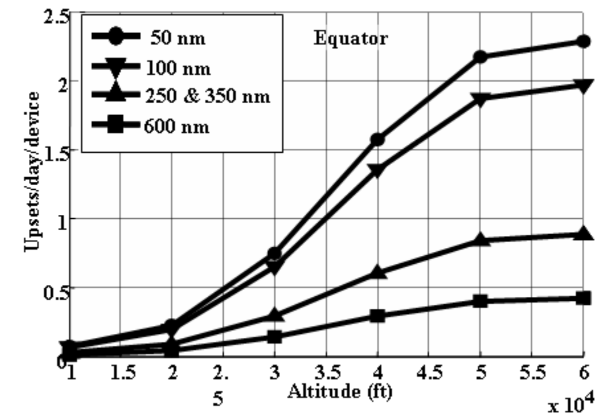

Figure 18. SER at equator computed by TSAREME for devices in Table 3.

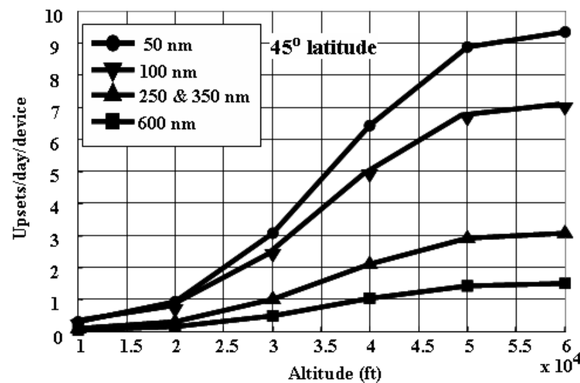

Figure 19.SER at 45 degrees latitude computed by TSAREME for devices in Table 3.

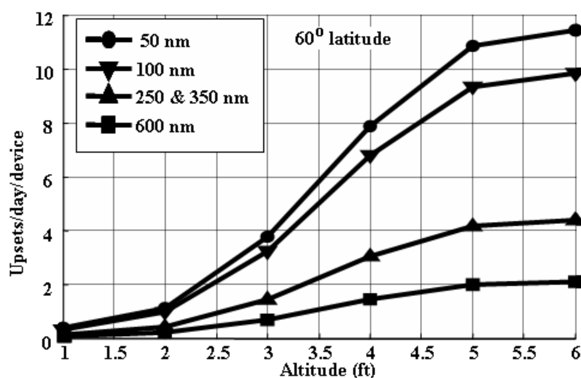

Figure 20. SER at 60 degrees latitude computed by TSAREME for devices in Table 3.

5. Summary and Conclusions

The Soft Error Rate (SER) produced by SEUs in microelectronic devices in space and in the atmosphere has been computed using a common model developed at Boeing, TSAREME. In space, TSAREME models protons, alphas, and heavy ions with atomic numbers up to 26 (iron) for GCR and peak solar flares. In the atmosphere, TSAREME computes the fluxes variations with latitude and longitude over the entire energy spectrum up to 10 GeV by methods already published.

In space, the SER was computed in two CMOS devices of similar structure. The first device is a 4 Mbit 2 micron CMOS memory. The second device was the first device with overlayers of aluminum and tantalum shielding and BPSG. A comparison of the SER generated for these devices indicated that metallic shielding and BPSG increased the SER from zero to 80 upsets per day in intense solar flares. In GCR, no SEUs were observed for either device.

In the atmosphere, the soft error rates due to atmospheric neutrons were computed in scaled submicron CMOS devices for various altitudes and latitudes. Model predictions of the SER for 350 and 600 nm CMOS representative of 1992 and 1994 were 3 and 1.8 upsets per day. Predictions of 9.8 and 11 upsets per day were made 100 and 50 nm CMOS devices representing the technologies of 2005 and 2011. These observations taken together indicate that the SER slowly increases with decreasing feature size for sizes below 100 nm.

Acknowledgements

The author would like to extend his gratitude to Mr. Robert A Robinson for inviting me to write a technical paper for the Huntsville chapter of IEEE, and both Mr. Robinson and Dr. T. K. Ramesh for their helpful suggestions in improving the manuscript. I would also wish to thank Mrs. Raija M. Dorrity for locating technical material in the Boeing Library, Dr. Gregg W. McKinney, Dr. Michael R. James, and Dr. Laurie Waters of Los Alamos National Laboratories for many help recommendations in developing the transport model inputs.

References

1. Premkishore Shivakumar, Michael Kistler, Steven W. Keckler, Doug Burger, Lorenzo Alvisi, "Modeling the Effect of Technology Trends on the Soft Error Rate of Combinatorial Logic", 2002 International Conference on Dependable Systems and Networks (DSN), June, 2002.
2. R. C. Baumann, 2005 *NSREC Short Course*, pp. II-1 to II-59.
3. S. Sotoh, Y. Tosaka, S. A. Wender, "Geometric effect of multiple-bit soft errors induced by cosmic ray neutrons on DRAM's." *Electron Device letters*, *IEEE*, Vol. 21, pp. 310-312, June, 2000.
4. R. Koga, S.H. Penzin, K.B. Crawford, and W.R. Crain, "Single event functional interrupt (SEFI) sensitivity in

microcircuits," *in Proc. 4Th RADECS*, pp. 311-318, Sept. 1997.
5. W.A. Kolasinski, J.B. Blake, J.K. Anthony, W.E. Price, E.C. Smith, "Simulation of cosmic-ray induced soft errors and latchup in integrated-circuit computer memories," *IEEE Trans. on Nuclear Science*, vol. NS-26, no. 6, pp. 5087-5091, 1979.
6. A.E. Waskiewicz, J.W. Groninger, V.H. Strahan, D.M. Long, "Burnout of power MOS transistors with heavy ions of Californium-252," *IEEE Trans. on Nuclear Science*, vol. 33, no. 6, pp. 1710-1713, 1986.
7. G.H. Johnson, J.H. Hohl, R.D. Schrimpf, K.F. Galloway, "Simulating single-event burnout in n-channel power MOSFETs," *IEEE Trans. on Electron Devices*, vol. 40, pp. 1001-1008, 1993.
8. T.A. Fischer, "Heavy-ion-induced, gate-rupture in power MOSFETs," *IEEE Trans. on Nuclear Science*, vol. 34, no. 6, pp. 1786-1791, 1987.
9. J.L. Titus, G.H. Johnson, R.D. Schrimpf, K.F. Galloway, "Single event burnout of power bipolar junction transistors," *IEEE Trans. on Nuclear Science*, vol. NS-38, no. 6, pp. 1315-1322, 1991.
10. D. Binder, E.C. Smith, A.B. Holman, "Satellite anomalies from galactic cosmic rays," *IEEE Trans. on Nuclear Science*, vol. NS-22, no. 6, pp. 2675-2680, Dec. 1975.
11. E. Normand, "Single Event Effects in Avionics", *IEEE Trans Nuc. Sci*., vol. 43, No. 2, 461, 1996.
12. Christina L. Howe, Robert A. Weller, Robert A. Reed, Marcus H. Mendenhall, Ronald D. Schrimpf, Kevin M. Warren, Dennis R. Ball, Lloyd W. Massengill, Kenneth A. LaBel, Jim W. Howard Jr., Nadim F. Haddad,"Role of Heavy-Ion Nuclear reactions in Determining On-Orbit Single Event Error Rates", *IEEE Trans. Nuc. Sci*., Vol. 52, No. 6, pp. 2182-2188, 2005.
13. http://www.ngdc.noaa.gov/stp/GOES/goes.html.
14. J. Feynman, G. Spitale and J Wang, "Interplanetary Proton Fluence Model" JPL 1991", *J. Geophys. Res*., 98, No. A8, 13281, 1993.
15. Allen J. Tylka, William F. Dietrich, Paul R. Boberg, Edward C. Smith, James H. Adams, Jr., *IEEE Trans. Nuc. Sci,* Vol. 43, no. 6, p 2758-2766, Dec. 1996.
16. P.P. Majewski, E. Normand, and D.L. Oberg, A New Solar Flare Heavy Ion Model and Its Implementation Through MACREE, An Improved Modeling Tool to Calculate Single Event Effects Rates in Space, *IEEE Trans. Nucl. Sci.* 42, 2043-2050 (1995).
17. J. L. Barth, C. S. Dyer, E. G. Strassinopoulos, "Space, Atmospheric, and Terrestrial Radiation Envionments", *IEEE Trans. Nuc. Sci*., Vo. 50, No. 3, 466, 2003.
18. A. Taber and E. Normand,"Single event upset in avionics", *IEEE Trans. Nuc. Sci,* Vol. 40, p. 120, Dec. 1993.
19. D. F. Smart and M. A. Shea, "Cosmic ray for shuttle altitudes derived from calculated cut-off rigidities", *Adv. Space Res*., vol. 4, no. 10, p. 161, 1984.
20. E. Normand and T. J. Baker, "Altitude and latitude variations in avionics SEU and atmospheric neutron flux", *IEEE Trans. Nuc. Sci*., vol. 40, p. 1484, 1993.
21. E. Normand, J. L. Wert, D. L. Oberg, P. P. Majewski, P. Voss, S. A. Wender, "Single Event Upset at Ground Level", *IEEE Trans. Nuc. Sci,* Vol. 43, p 2743-2754, 1997.
22. J. H. Adams, R. Silberberg, and G. D. Badhwar, 'Calculation of the Vavilov Distribution', *Nucl. Inst. Meth*., Vol. 124, p. 551-556, 1975.
23. Michael R. James, G. W. McKinney, John S. Hendricks, Michael Moyers, 'Recent enhancements in MCNPX: Heavy-ion transport and the LAQGSM physics model', *Nuc. Instruments and Methods in Phys. Research*, A, 562, pp. 819-822, 2006.
24. G.C. Messenger, M.S. Ash, *The Effects of Radiation on Electronic Systems*, 2nd edition, Van Nostrand Reinhold, NY, 1992.
25. http://www.mathworks.com/products/
26. J. L. Zeigler and W. A. Lanford, "Effect of Cosmic Rays on Computer memories", Science, 206, 776, November 1979.

27. Eugene Normand, Jerry L. Wert, and W. Ross Doherty, Dennis L. Oberg, Paul R. Measel, Tommy L. Christell, "Use of PbBe source to simulate neutron single event upsets in static RAMs, *IEEE Trans Nuc. Sci*., vol. 35, No. 6, 1523-1528, 1988.
28. John R. Letaw, Eugene Normand, "Guidelines for predicting single event upsets in neutron environments", *IEEE Trans Nuc. Sci*., vol. 36, No. 6, 1500-1506, 1991.
29. Kevin M. Warren, Robert A. Weller, Marcus Mendenhall, Robert A. Reed, Dennis R. Ball, Christina L. Howe, Brian D. Olson, Michael L. Alles, Lloyd W. Messengill, Ronald D. Schrimpff, Nadim F. Haddad, Scott E. Doyle, Dale McMorrow, Joseph S. Melinger, William T. Lotshaw, "Contribution of Nuclear Reactions to Heavy Ion Single Event Upset Cross-Section Measurements in a High-Density SEU Hardened SRAM".
30. http://www.wilmad-labglass.com/pdf/Borosilicate%20Glass%20Properties.pdf
31. P. Robinson, W. Lee, R. Aguero, S. Gabriel, "Anomalies due to single event upsets," *Journal of Spacecraft and Rockets*, vol. 31, no. 2, pp. 166-171, Mar-Apr 1994.